

Polarization impact on sensitivity of Rydberg atom-based microwave sensors

Minghao Cai(蔡明皓), Aomao Wei(魏奥贸), Shanshan Chen(陈珊珊), and Yuming Huang(黄聿铭)
Citation: Chin. Phys. B, 2025, 34 (**8**): 083201. DOI: 10.1088/1674-1056/add005
http://cpb.iphy.ac.cn; http://iopscience.iop.org/cpb

What follows is a list of articles you may be interested in

Optimization strategies for operational parameters of Rydberg atom-based amplitude modulation receiver

Yuhao Wu(吴宇豪), Dongping Xiao(肖冬萍), Huaiqing Zhang(张淮清), and Sheng Yan(阎晟)
Chin. Phys. B, 2025, 34 (**1**): 013201. DOI: 10.1088/1674-1056/ad886a

Microwave field sensor based on cold cesium Rydberg three-photon electromagnetically induced spectroscopy

Yuan-Yuan Wu(吴圆圆), Yun-Hui He(何云辉), Yue-Chun Jiao(焦月春), and Jian-Ming Zhao(赵建明)
Chin. Phys. B, 2024, 33 (**11**): 113201. DOI: 10.1088/1674-1056/ad7579

Electric field intensity measurement by using doublet electromagnetically induced transparency of cold Rb Rydberg atoms

Ting Gong(宫廷), Shuai Shi(师帅), Zhonghua Ji(姬中华), Guqing Guo(郭古青), Xiaocong Sun(孙小聪), Yali Tian(田亚莉), Xuanbing Qiu(邱选兵), Chuanliang Li(李传亮), Yanting Zhao(赵延霆), and Suotang Jia(贾锁堂)
Chin. Phys. B, 2023, 32 (**10**): 103202. DOI: 10.1088/1674-1056/acf120

Atom-based power-frequency electric field measurement using the radio-frequency-modulated Rydberg spectroscopy

Weixin Liu(刘伟新), Linjie Zhang(张临杰), and Tao Wang(汪涛)
Chin. Phys. B, 2023, 32 (**5**): 053203. DOI: 10.1088/1674-1056/aca6db

High-precision three-dimensional Rydberg atom localization in a four-level atomic system

Hengfei Zhang(张恒飞), Jinpeng Yuan(元晋鹏), Lirong Wang(汪丽蓉), Liantuan Xiao(肖连团), and Suo-tang Jia(贾锁堂)
Chin. Phys. B, 2021, 30 (**5**): 053202. DOI: 10.1088/1674-1056/abd46f

---

Polarization impact on sensitivity of Rydberg atom-based microwave sensors

Minghao Cai(蔡明皓)[1,2], Aomao Wei(魏奥贸)[1], Shanshan Chen(陈珊珊)[1], and Yuming Huang(黄聿铭)[1,†]

[1] *College of Photoelectronic Engineering, Chongqing University of Posts and Telecommunications, Chongqing* 400065, *China*
[2] *Chongqing Integrated Circuit Collaborative Innovation Center, Chongqing* 401332, *China*

(Received 19 December 2024; revised manuscript received 25 March 2025; accepted manuscript online 24 April 2025)

We investigate the sensitivity of a Rydberg atom-based microwave sensor under two polarization configurations as a function of local oscillator (LO) microwave field strength. By employing parallel and perpendicular alignments of laser and microwave polarizations in our experimental setup, we study the Autler–Townes (AT) splitting spectrum and optical response of probe transmission, and analyze their sensing effects. The results show that the parallel polarization configuration offers higher gain and better sensitivity than the perpendicular configuration. We achieve a sensitivity of 4.150(69) $\mathrm{nV\cdot cm^{-1}\cdot Hz^{-1/2}}$ at an LO microwave field strength of 1.74 mV/cm. This work demonstrates the significant role of polarization alignment on the performance of Rydberg atom-based microwave sensors.

Keywords: Rydberg atom, microwave sensing, polarization configuration, sensitivity

PACS: 32.80.Ee, 42.50.Gy, 07.57.Kp

DOI: 10.1088/1674-1056/add005 **CSTR:** 32038.14.CPB.add005

1. Introduction

In recent years, an emerging type of sensor employing atoms in Rydberg states has made significant progress,[1–7] due to their large transition dipole moments and high susceptibility to applied electromagnetic fields.[8] This optical sensor based on Rydberg electromagnetically induced transparency (EIT) spectroscopy and Autler–Townes (AT) splitting has been employed to detect and receive radio frequency (RF) field[9,10] with a wide frequency range from 100 MHz to 1 THz.[11–16] Particularly, Rydberg atom-based sensors has shown excellent capability in RF measurement including amplitude,[13,17–19] polarization,[20,21] and phase.[6,22–24] In addition, wireless communication receivers have been implemented using Rydberg atom-based sensor, including amplitude modulation (AM), frequency modulation (FM), phase modulation (PM), and digital modulation signals.[9,25–33]

Sensitivity measurement of RF electric fields is a major focus in the development of atombased sensors.[34–40] Various methods have been proposed to improve the minimal detectable field and sensitivity. For example, Simons *et al.* achieved a twofold improvement in measurement sensitivity by detuning the RF frequency, compared to conventional on-resonance AT splitting measurements.[41] Jia *et al.* demonstrated that auxiliary microwave-dressed Rydberg atoms can extend the electrometric span from mV/cm to μV/cm.[16] Sedlacek *et al.* achieved a sensitivity of 30 $\mathrm{\mu V\cdot cm^{-1}\cdot Hz^{-1/2}}$ by using the bright resonance of EIT.[42] Jing *et al.* greatly improved the sensitivity to 55 $\mathrm{nV\cdot cm^{-1}\cdot Hz^{-1/2}}$ with the method of Rydberg[6] atom superheterodyne reception. In our previous work, we optimized a series of experimental parameters at microwave resonance and increased the measurement sensitivity to 5.102(49) $\mathrm{nV\cdot cm^{-1}\cdot Hz^{-1/2}}$.

Most techniques for improving measurement sensitivity, as well as those used in Rydberg atom-based wireless communication,[6,31,43] rely on the EIT transmission optical response to the applied RF field. Researchers typically employed nD to n'P microwave transitions to achieve higher detection sensitivity, which have larger dipole moments and transmission signals.[2,6,19] However, the performance of nD to n'P transitions are highly sensitive to laser polarization.[44,45] The magnetic substructure of the atom may result in only partial coupling with microwave fields during these transitions, leading to a characteristic spectroscopic signature of a pair of microwave-coupled AT peaks and a center peak that does not respond to the microwave.[21,22,32] In this case, the EIT-AT probe transmission is dependent on the relative polarizations of the laser and microwave fields, and can be approximated as[21]

$$T = 1 - \cos^2(\xi)\sin^2(\zeta), \tag{1}$$

where ξ is the relative angle between the microwave vector and laser polarization, ζ is the angle between the microwave vector and the laser path. This dependence affects both the dipole moment and the optical response, causing a reduction in sensitivity. The relative mechanisms of polarization sensitivity on detection performance require further exploring.

We study the microwave transition $81D_{5/2} \leftrightarrow 82P_{3/2}$ under two different polarization configurations in order to inves-

†Corresponding author. E-mail: huangym@cqupt.edu.cn

© 2025 Chinese Physical Society and IOP Publishing Ltd. All rights, including for text and data mining, AI training, and similar technologies, are reserved.

tigate the influence of laser polarization on the sensitivity measurement of Rydberg atom-based sensor. The probe and coupling lasers polarizations are aligned parallel to the microwave polarization, while in the other case, they are aligned perpendicularly to the microwave polarization. We analyze their response to weak microwave fields and measure the corresponding sensitivities. This work aids in selecting appropriate microwave transitions for Rydberg atom-based sensors.

2. Experiment and theory

Two different experimental configurations and their corresponding energy transitions are shown in Fig. 1. Figure 1(a) represents the experimental configuration with laser polarization parallel to the microwave polarization, and figure 1(b) represents the experimental configuration with laser polarization perpendicular to the microwave polarization. In both experimental configurations, the probe laser (with a $1/e^2$ -waist radius of 750 μm) and the coupling laser (with a $1/e^2$-waist radius of 1.25 mm) counter-propagate through a cylindrical room-temperature Rb cell measuring 25 mm in diameter and 75 mm in length. The probe laser couples the ground state $5S_{1/2}$ to the intermediate state $5P_{3/2}$, while the coupling laser drives the transition from the intermediate state $5P_{3/2}$ to the high Rydberg state $81D_{5/2}$, forming a ladder-type EIT configuration. A high-speed photodiode detector (PD) records the transmission spectrum of the probe laser, which is monitored using a digital oscilloscope. A local oscillator (LO) microwave field at a frequency of 3.866 GHz is generated using a horn antenna to resonate with the transition $81D_{5/2} \leftrightarrow 82P_{3/2}$.

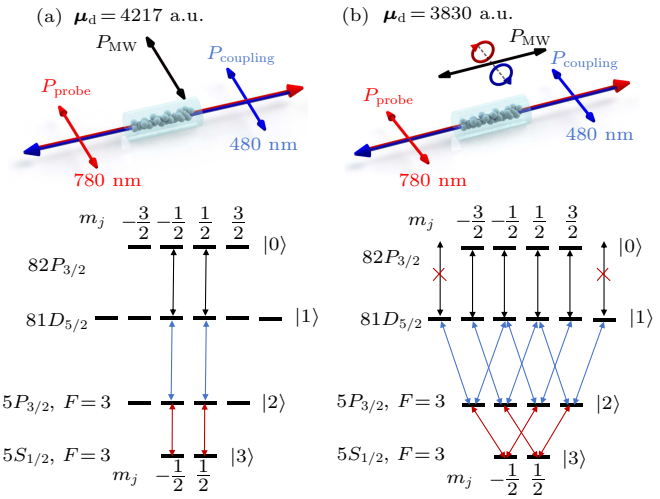


Fig. 1. Experimental configuration diagrams showing the laser and microwave polarizations: (a) laser polarizations parallel to the microwave polarization, and (b) laser polarizations perpendicular to the microwave polarization, along with the corresponding energy level transition. P_{probe}, $P_{coupling}$, and P_{MW} denote the polarization directions of the probe laser, coupling laser, and microwave field, respectively.

To eliminate the influence of Doppler broadening in the EIT spectrum, we lock the probe laser at 780 nm and scan the coupling laser frequency around 480 nm to record the spectrum more precisely. The probe laser is a cat-eye laser from Moglabs operating at 780.246 nm, with a maximum output power of 180 mW and a free-running linewidth of approximately 1 MHz. The coupling laser is provided by a frequency-doubled amplified diode laser system (TA-SHGpro, Toptica, Munich, Germany), which is scanned across the $5P_{3/2} \leftrightarrow 81D_{5/2}$ transition and monitored in real time by a Fabry–Pérot (FP) cavity for relative frequency referencing. The probe laser intensity of 100 μW and the coupling laser intensity of 130 mW were used.

Due to the specific polarization directions of the laser and microwave electric fields, the detailed magnetic substructure of the atoms should be considered. As shown below in Fig. 1, we denote the overall hyperfine levels ($|5S_{1/2}, F=3\rangle$ and $|5P_{3/2}, F=3\rangle$) while representing the sublevels in terms of the electron angular momentum projection, m_j. This approach is justified by the fact that optical transitions predominantly involve changes in m_j, with the nuclear spin projection, m_I, remaining essentially unchanged ($\Delta m_I \approx 0$). Consequently, each state labeled by a particular m_j actually corresponds to a linear combination of $|m_j, m_I\rangle$ basis states that together form the complete $|F, m_F\rangle$ eigenstate. Although this representation is an approximation, it facilitates a clearer interpretation of polarization-dependent selection rules and transition probabilities.

We denote ω_{n,m_j} as the energy of the specific magnetic sublevel, where $n = 0$, 1 corresponds to the two microwave-coupled Rydberg states, and $n = 2$, 3 corresponds to the intermediate state $|5P_{3/2}, F=3\rangle$ and the ground state ($|5S_{1/2}, F=3\rangle$. Here, m_j ($m_j = \pm 1/2, \pm 3/2, \pm 5/2$) represents the magnetic sublevels. The Hamiltonian of the system can be expressed as

$$H = H_1 + H_0. \tag{2}$$

Here H_0 is the Hamiltonian of the unperturbed atom, given by

$$H_0 = \begin{bmatrix} \omega_{0,3/2} & 0 & \cdots & 0 \\ 0 & \omega_{0,1/2} & \cdots & 0 \\ \vdots & \vdots & \ddots & \vdots \\ 0 & 0 & \cdots & \omega_{3,-1/2} \end{bmatrix}, \tag{3}$$

and H_1 describes the interactions between the laser and the atom

$$H_1 = -\frac{h}{2} \begin{bmatrix} 0 & V_{0,3/2,0,1/2} & \cdots & V_{0,3/2,3,-1/2} \\ V^*_{0,3/2,0,1/2} & 0 & \cdots & V_{0,1/2,3,-1/2} \\ \vdots & \cdots & \ddots & \vdots \\ V^*_{0,3/2,3,-1/2} & V^*_{0,1/2,3,-1/2} & \cdots & 0 \end{bmatrix}, \tag{4}$$

where V_{n,m_j,n',m'_j} represents the interaction between the energy states $|n, m_j\rangle$ and $|n', m'_j\rangle$. According to transition selection rules, when $\Delta n = n - n' \neq 1$, we have $V_{n,m_j,n',m'_j} = 0$.

In the experimental configuration shown in Fig. 1(a), the probe laser, coupling laser, and microwave field are all linearly polarized along the same direction. Therefore, all transitions are π-polarized, allowing only transitions with $\Delta m_j = 0$. The interaction matrix elements are given by $V_{n,m_j,n',m'_j} = \Omega_{n,m_j,n',m'_j} e^{i\omega_i t}$ when $\Delta m_j = 0$, while all other interaction matrix elements are zero. Here, Ω_{n,m_j,n',m'_j} is the Rabi frequency, and ω_i is the angular frequency of the corresponding transition between magnetic sublevels. However, in the perpendicular polarization configuration shown in Fig. 1(b), the probe and coupling lasers are polarized perpendicular to the microwave polarization. In this case, the laser polarizations can be considered as a superposition of σ^+ and σ^- polarizations relative to the quantization axis defined by the microwave field, allowing only transitions with $\Delta m_j = \pm 1$. For transitions $5S_{1/2} \leftrightarrow 5P_{3/2} \leftrightarrow 81D_{5/2}$, the interaction matrix elements are $V_{n,m_j,n',m'_j} = \Omega_{n,m_j,n',m'_j} e^{i\omega_i t}$ when $\Delta m_j = \pm 1$ and are zero for all other Δm_j. The microwave field, still being π-polarized, only allows transitions with $\Delta m_j = 0$. This leads to a critical difference as illustrated in the below of Fig. 1: in the perpendicular configuration, atoms are optically pumped to the outermost magnetic sublevels $m_j = \pm 5/2$ in the $81D_{5/2}$ state. Since the microwave field only allows $\Delta m_j = 0$ transitions, and there are no corresponding $m_j = \pm 5/2$ sublevels in the $82P_{3/2}$ state (which has $m_j = \pm 3/2$ as its outermost levels), the microwave transition from $81D_{5/2}$ to $82P_{3/2}$ is forbidden for these outermost sublevels. Consequently, the microwave coupling is less effective in the perpendicular configuration.

Both experimental configurations can yield steady-state solutions using the density matrix method[42,46] under the rotating wave approximation (RWA). The Hamiltonian can be considered time-independent as

$$\frac{d\rho}{dt} = -\frac{i}{\hbar}[H,\rho] + L_d, \tag{5}$$

where L_d represents the dephasing and decay terms in Lindblad form. In the experimental configuration with parallel polarizations, the microwave transition dipole moment is $\mu_d = 4217$ a.u. However, the energy level transitions become more complex in the configuration where the laser polarizations are perpendicular to the microwave polarization. The calculation of the dipole moment requires considering the transition probabilities of each magnetic sublevel, resulting in an effective microwave transition dipole moment $\mu_d = 3830$ a.u. This difference affects the coupling strength between the microwave field and the atomic system, thereby influencing the measured signal strength and the sensitivity of the sensor.

3. Results and discussion

Figure 2(a) shows the experimentally measured EIT-AT splitting spectrum when the laser polarizations are parallel to the microwave polarization. A pronounced Autler–Townes splitting is observed at the resonance frequency, indicating strong coupling between the Rydberg states $81D_{5/2}$ and $82P_{3/2}$ mediated by the microwave field. The splitting width increases with the microwave power, demonstrating the expected dependence on the microwave field strength. The corresponding theoretical simulation is presented in Fig. 2(b). The simulation is based on the density matrix equations described earlier, incorporating the relevant transition dipole moments and considering only transitions with $\Delta m_j = 0$, as dictated by the selection rules for π-polarized laser in this configuration. The theoretical spectrum closely matches the experimental data, validating our theoretical model and confirming that the system behavior is well described under these conditions.

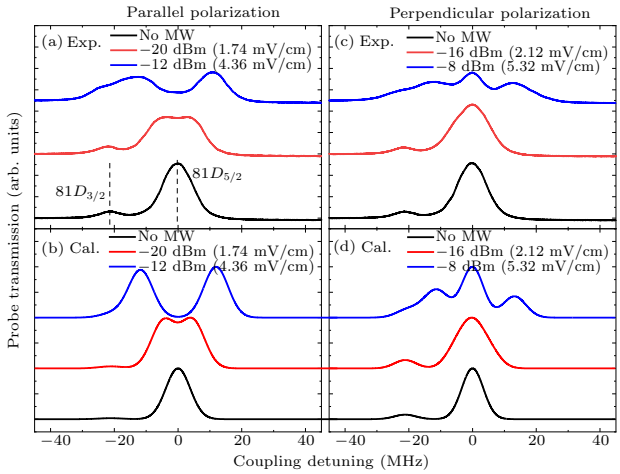


Fig. 2. (a) Experimental EIT-AT splitting spectrum with laser polarizations parallel to the microwave polarization; (b) corresponding theoretical simulation. (c) Experimental EIT-AT spectrum with laser polarizations perpendicular to the microwave polarization, showing a central peak and side peaks; (d) corresponding theoretical simulation. The main peak at zero detuning corresponds to $81D_{5/2}$ Rydberg EIT, and the small one at -21 MHz results from $81D_{3/2}$ EIT.

Figure 2(c) displays the EIT-AT splitting spectrum when the laser polarizations are perpendicular to the microwave polarization. In this configuration, the EIT spectrum exhibits a characteristic structure consisting of a central peak that does not respond to the microwave field and a pair of Autler–Townes (AT) split peaks on either side. This phenomenon occurs because atoms are excited to the $m_j = \pm 5/2$ sublevels of the $81D_{5/2}$ state via the probe and coupling laser transitions with $\Delta m_j = \pm 1$, and the π-polarized LO microwave field cannot induce transitions from these $m_j = \pm 5/2$ sublevels, as illustrated in the energy level transitions in Fig. 1(b). Consequently, atoms accumulate in these outermost magnetic sublevels, which do not participate in the microwave coupling to the $82P_{3/2}$ state. The central peak corresponds to transitions involving the $m_j = \pm 5/2$ sublevels that remain unaffected by the microwave field, while the side peaks result from the microwave-coupled transitions between magnetic sublevels with $m_j = \pm 1/2$ and $m_j = \pm 3/2$. The presence

of both microwave-coupled and uncoupled transitions leads to the observed spectral structure. The corresponding theoretical simulation is presented in Fig. 2(d), incorporating the specific selection rules and polarization dependencies discussed above. It reproduces the experimental spectrum, including the central peak and the AT-split side peaks. The agreement between the theoretical and experimental results confirms the validity of our theoretical model and enhances our understanding of the underlying physical mechanisms in the perpendicular polarization configuration.

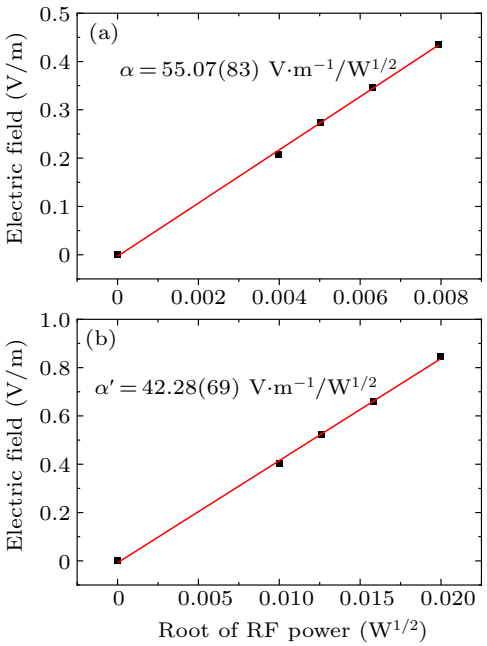


Fig. 3. Calibration of the LO microwave field strength using the standard antenna method for (a) parallel polarization and (b) perpendicular polarization configurations.

To quantify the effect of the polarization configurations on microwave field sensing, it is necessary to calibrate the microwave horn antenna under both experimental configurations. The standard antenna method is commonly employed to calibrate the LO microwave field E_{LO}, which is expressed by the following equation:[6]

$$E_{\mathrm{LO}} = \sqrt{\frac{\eta g \alpha_1 P_{\mathrm{RF}}}{4\pi d^2}}, \tag{6}$$

where η is the free space impedance ($\eta = 377\ \Omega$), g is the gain of the horn antenna, α_1 represents the loss between the microwave source and the horn antenna, P_{RF} is the input power of the microwave source, and d is the distance between the horn antenna and the receiving point. Since all these coefficients are constants, equation (6) can be reduced as

$$E_{\mathrm{LO}} = \alpha\sqrt{P_{\mathrm{RF}}}, \tag{7}$$

where $\alpha = \sqrt{\eta g \alpha_1/(4\pi d^2)}$ is the calibration factor of horn antenna. The E_{LO} can be calculated by the AT splitting Δ_{RF} as described as[42]

$$E_{\mathrm{LO}} = \frac{2\pi\hbar}{\mu_{\mathrm{d}}}\Delta_{\mathrm{RF}}. \tag{8}$$

A series of data points were collected at different microwave powers under both experimental configurations, as shown by the black squares in Fig. 3. The calibration factors α and were α' determined through linear fitting of these data points, represented by the red solid lines. The calibration factor for the parallel polarization configuration was found to be $\alpha = 55.07(83)\ \mathrm{V\cdot m^{-1}/W^{1/2}}$, while for the perpendicular polarization configuration, it is $\alpha' = 42.28(69)\ \mathrm{V\cdot m^{-1}/W^{1/2}}$. The difference in calibration factors arises because adjusting the polarization configuration necessitates repositioning the horn antenna. As a result, a weaker E_{LO} is obtained, as deduced from Eq. (7) for a given attenuated microwave power.

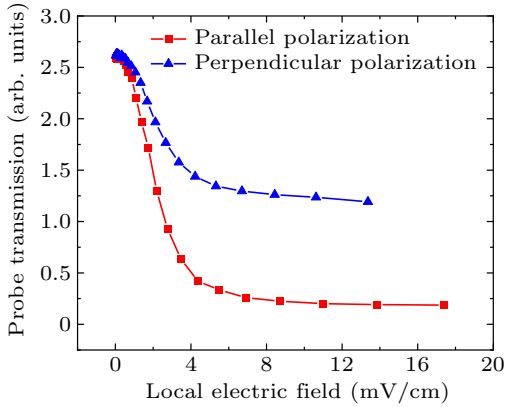


Fig. 4. The probe transmission response as a function of the LO microwave field for both experimental configurations.

We further investigate the optical response dependent on the LO field. The probe transmission intensity at the center of the EIT-AT splitting spectrum is measured under different LO microwave field strengths, as shown in Fig. 4. The slope of the transmission curve reflects the sensitivity of probe optical response to the applied microwave power. In both experimental configurations, at low microwave power, the AT splitting is very small, rendering the probe optical response insensitive to the microwave field. Conversely, at very high microwave power, the AT splitting has already been separated, which also leads to a decreased sensitivity in the probe optical response. Therefore, there exists an optimal LO microwave field strength at an intermediate value where the sensitivity is maximized. From Fig. 4, it can be seen that this optimal field strength is around 2 mV/cm. At the optimal LO field, the parallel configuration maintains the maximum slope, indicating the highest optical response gain. However, the perpendicular configuration exhibits a significantly reduced dynamic response due to the presence of a central peak that does not respond to the microwave field, which diminishes the overall sensitivity. These observations highlight the critical influence of the polarization configuration on the sensitivity measurements

in Rydberg-atom-based microwave sensors. The polarization-dependent coupling efficiency affects the dynamic optical response of the probe light, directly impacting the sensor's performance in detecting microwave fields.

We conducted measurements for both polarization configurations to compare the gain coefficients and the corresponding detection sensitivities under different LO microwave field strengths ranging from 0.6 mV/cm to 5.5 mV/cm, as presented in Fig. 5. The gain G is defined as the inverse of the conversion coefficient κ ($G = 1/\kappa$), where κ represents the conversion from the applied electric field to the photodetector (PD) voltage signal. The detailed process for calculating the sensitivity and gain coefficients has been thoroughly described in our previous work.[43] Briefly, the weak RF electric field is transmitted to the atomic RF-optical response through amplitude modulation (AM) of the LO field. By applying an AM signal to the LO field and measuring the corresponding modulation in the probe transmission, the relationship between the applied electric field and the PD voltage response is established. In our current measurements, instead of using κ directly, we use its inverse G to represent the gain, as a larger gain indicates higher sensitivity.

As shown in Fig. 5(a), the gain reaches a maximum at an intermediate LO field for both polarization configurations, corresponding to the optimal operating point where the sensor exhibits the highest sensitivity around 2 mV/cm. Notably, the gain in the parallel polarization configuration is significantly higher than in the perpendicular configuration across the range of LO field strengths, reflecting the enhanced coupling efficiency due to polarization alignment. Figure 5(b) presents the corresponding detection sensitivities calculated based on the measured noise-equivalent power and the signal-to-noise ratio of the system. The sensitivity is inversely related to the gain G, meaning that a higher gain leads to a lower minimum detectable electric field. The parallel configuration achieves superior sensitivity compared to the perpendicular configuration, which is consistent with the observed differences in gain.

Specifically, in the parallel polarization configuration, the Rydberg-atom microwave sensing system achieves its best detection sensitivity at an LO field strength of 1.74 mV/cm, with a sensitivity of $S = 4.150\,(69)\ \mathrm{nV\cdot cm^{-1}\cdot Hz^{-1/2}}$. This sensitivity surpasses the previously reported value of $S = 5.102(49)\ \mathrm{nV\cdot cm^{-1}\cdot Hz^{-1/2}}$ obtained with atoms in the $78S_{1/2}$ Rydberg state.[43] The improvement is attributed to the larger microwave transition dipole moment of 4217 a.u. for the $81D_{5/2} \leftrightarrow 82P_{3/2}$ transition, compared to 2998 a.u. for the $78S_{1/2} \leftrightarrow 78P_{3/2}$, as well as the higher probe transmission intensity of the $81D_{5/2}$ EIT spectrum in the absence of the LO field.

In contrast, in the perpendicular polarization configuration, the best detection sensitivity is achieved at an LO field strength of 2.12 mV/cm, with a sensitivity of $S = 15.07\,(14)\ \mathrm{nV\cdot cm^{-1}\cdot Hz^{-1/2}}$. This sensitivity is significantly lower than that of the parallel configuration, highlighting the substantial impact of the relative polarization alignment between the laser and microwave fields on the sensor's performance. The presence of a non-responsive central peak in the perpendicular configuration reduces the overall dynamic response and limits the achievable sensitivity.

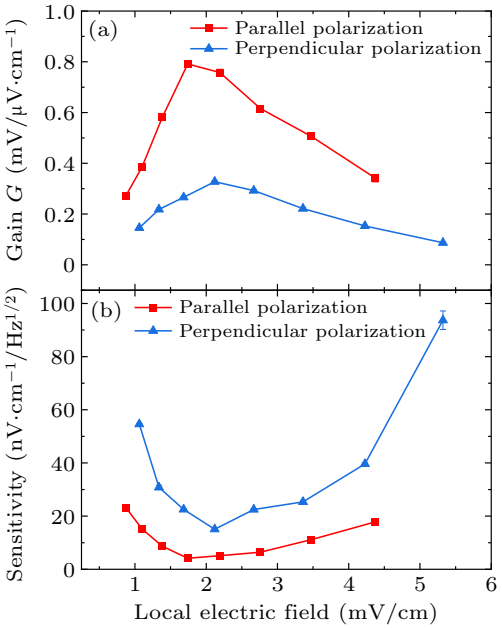


Fig. 5. (a) Optical response gain G as a function of the LO microwave field strengths ranging from 0.6 mV/cm to 5.5 mV/cm for both parallel (red line) and perpendicular (blue line) polarization configurations. (b) Corresponding detection sensitivities S calculated for both configurations.

4. Conclusions

In summary, we have investigated the sensitivity of Rydberg atom-based sensor under different polarization configurations and LO field strengths. By comparing the parallel and perpendicular configurations, it demonstrated that the relative polarization alignment significantly influences the microwave coupling efficiency and the sensor's performance. The parallel configuration achieved a superior detection sensitivity of $S = 4.150\,(69)\ \mathrm{nV\cdot cm^{-1}\cdot Hz^{-1/2}}$ at an LO field strength of 1.74 mV/cm, where polarization alignment allows for complete coupling between the magnetic sublevels of the energy levels. By comparison, the perpendicular configuration exhibited a reduced sensitivity of $15.07\,(14)\ \mathrm{nV\cdot cm^{-1}\cdot Hz^{-1/2}}$ at 2.12 mV/cm, attributed to diminished coupling efficiency and the presence of a non-responsive central peak in the EIT-AT splitting spectrum. These findings underscore the critical role of polarization alignment between the laser and microwave fields in optimizing sensor performance, providing valuable insights for the development of high-sensitivity microwave sensing technologies based on Rydberg atoms.

Acknowledgements

Project supported by the Natural Science Foundation of Chongqing, China (Grant Nos. CSTB2024NSCQ-MSX0880 and CSTB2024NSCQ-MSX1187) and the Fund from Chongqing University of Posts and Telecommunications (Grants Nos. A2024-33 and A2023-54).

References

[1] Yuan S X, Jing M Y, Zhang H, Zhang L J, Xiao L T and Jia S T 2024 *Opt. Express* **32** 8378
[2] Li L, Jiao Y C, Hu J L, Li H Q, Shi M, Zhao J M and Jia S T 2023 *Opt. Express* **31** 29228
[3] Borówka S, Pylypenko U, Mazelanik M and Parniak M 2023 *Nat. Photonics* **18** 32
[4] Holloway C L, Gordon J A, Jefferts S, Schwarzkopf A, Anderson D A, Miller S A, Thaicharoen N and Raithel G 2014 *IEEE Trans. Antennas Propag.* **62** 6169
[5] Fan H Q, Kumar S, Sedlacek J, Kübler H, Karimkashi S and Shaffer J P 2015 *J. Phys. B* **48** 202001
[6] Jing M Y, Hu Y, Ma J, Zhang H, Zhang L J, Xiao L T and Jia S T 2020 *Nat. Phys.* **16** 911
[7] Prajapati N, Robinson A K, Berweger S, Simons M T, Artusio-Glimpse A B and Holloway C L 2021 *Appl. Phys. Lett.* **119** 214001
[8] Meyer D H, Hill J C, Kunz P D and Cox K C 2023 *Phys. Rev. Appl.* **19** 014025
[9] Gallagher T F 1994 *Rydberg Atom* (Cambridge: Cambridge University Press)
[10] Holloway C L, Simons M T, Abdulaziz H, Gordon J A, Anderson D A, Raithel G and Voran S 2021 *IEEE Antenna Propag. Mag.* **63** 63
[11] Zhang L J, Jia Y, Jing M Y, Guo L P, Zhang Hao, Xiao L T and Jia S T 2019 *Laser Phys.* **29** 035701
[12] Liu B, Zhang L H, Liu Z K, Zhang Z Y, Zhu Z H, Gao W, Guo G C, Ding D S and Shi B S 2022 *Phys. Rev. Appl.* **18** 014045
[13] Hu J L, Li H Q, Song R, Bai J X, Jiao Y C, Zhao J M and Jia S T 2022 *Appl. Phys. Lett.* **121** 014002
[14] Gordon J A, Holloway C L, Schwarzkopf A, Anderson D A, Miller S, Thaicharoen N and Raithel G 2014 *Appl. Phys. Lett.* **105** 024104
[15] Downes L A, MacKellar A R, Whiting D J, Bourgenot C, Adams C S and Weatherill K J 2020 *Phys. Rev. X* **10** 011027
[16] Jia F D, Liu X B, Mei J, Yu Y H, Zhang H Y, Lin Z Q, Dong H Y, Zhang J, Xie F and Zhong Z P 2021 *Phys. Rev. A* **103** 063113
[17] Simons M T, Gordon J A and Holloway C L 2018 *Appl Opt.* **57** 6456
[18] Liu W X, Zhang L J and Wang T 2023 *Chin. Phys. B* **32** 053203
[19] Gordon J A, Simons M T, Haddab A H and Holloway C L 2019 *AIP Adv.* **9** 045030
[20] Hao L P, Xue Y M, Fan J B, Bai J X, Jiao Y C and Zhao J M 2020 *Chin. Phys. B* **29** 033201
[21] Sedlacek J A, Schwettmann A, Kubler H and Shaffer J P 2013 *Phys. Rev. Lett.* **111** 063001
[22] Song Z F, Zhang W F, Wu Q, Mu H H, Liu X C, Zhang L J and Qu J F 2018 *Sensors* **18** 3205
[23] Holloway C L, Simons M T, Gordon J A and Novotny D 2019 *IEEE Antennas Wireless Propag. Lett.* **18** 1853
[24] Simons M T, Haddab A H, Gordon J A, Novotny D and Holloway C L 2019 *IEEE Access* **7** 164975
[25] Gordon J A, Simons M T, Haddab A H and Holloway C L 2019 *AIP Adv.* **9** 045030
[26] Deb A B and Kjrgaard N 2018 *Appl. Phys. Lett.* **112** 211106
[27] Tretiakov A, Potts C A, Lee T S, Thiessen M J, Davis J P and LeBlanc L J 2020 *Appl. Phys. Lett.* **116** 164101
[28] Zou H Y, Song Z F, Mu H H, Feng Z G, Qu J F and Wang Q L 2020 *Appl. Sci.* **10** 1346
[29] Simons M T, Haddab A H, Gordon J A and Holloway C L 2019 *International Symposium on Electromagnetic Compatibility*, September 2–6, 2019, Barcelona, Spain, p. 885
[30] Song Z F, Zhang W F, Liu X C, Zou H Y, Zhang J, Jiang Z Y and Qu J F 2018 *IEEE Globecom Workshops*, December 9–13, 2018, Abu Dhabi, United Arab Emirates, p. 1
[31] Song Z F, Liu H P, Liu X C, Zhang W F, Zou H Y, Zhang J and Qu J F 2019 *Opt. Express* **27** 8848
[32] Anderson D A, Sapiro R E and Raithel G 2021 *IEEE Trans. Antenna Propag.* **69** 2455
[33] Li H Q, Hu J L, Bai J X, Shi M, Jiao Y C, Zhao J M and Jia S T 2022 *Opt. Express* **30** 13522
[34] Yang K, Mao R Q, He L, Yao J W, Li J B, Sun Z S and Fu Y Q 2023 *EPJ Quantum Technol.* **10** 23
[35] Wu B, Zhou Y L, Ding Z K, Mao R Q, Qian S X, Wan Z Q, Liu Y, An Q, Lin Y and Fu Y Q 2024 *EPJ Quantum Technol.* **11** 30
[36] Fan H Q, Kumar S, Daschner R, Kubler H and Shaffer J P 2014 *Opt. Lett.* **39** 3030
[37] Li S H, Yuan J P and Wang L R 2020 *Appl. Sci.* **10** 8110
[38] Liu X B, Jia F D, Zhang H Y, Mei J, Yu Y H, Liang W C, Zhang J, Xie F and Zhong Z P 2021 *AIP Adv.* **11** 085127
[39] Li S H, Yuan J P, Wang L R, Xiao L T and Jia S T 2022 *Front. Phys.* **10** 846687
[40] Holloway C T, Prajapati N, Artusio-Glimpse A B, Berweger S, Simons M T, Kasahara Y, Alù A and Ziolkowski R W 2022 *Appl. Phys. Lett.* **120** 204001
[41] Simons M T, Gordon J A, Holloway C L, Anderson D A, Miller S A and Raithel G 2016 *Appl. Phys. Lett.* **108** 174101
[42] Sedlacek J A, Schwettmann A, Kübler H, Löw R, Pfau T and Shaffer J P 2012 *Nat. Phys.* **8** 819
[43] Cai M H, You S H, Zhang S S, Xu Z S and Liu H P 2023 *Appl. Phys. Lett.* **122** 161103
[44] McGloin D, Dunn M H and Fulton D J 2000 *Phys. Rev. A* **62** 053802
[45] Chen Y C, Lin C W and Yu I A 2000 *Phys. Rev. A* **61** 053805
[46] Fan H Q, Kumar S, Kübler H and Shaffer J P 2016 *J. Phys. B: At. Mol. Opt. Phys.* **49** 104004